Porosity evolution in tight gas sands of the Upper Triassic Xujiahe Formation, western Sichuan basin, China

Dongxia Chen[1,*], Xiongqi Pang[1], Liang Xiong[2], Lei Wang[1], and Mingxian Xie[1]

[1] State Key Laboratory of Petroleum Resource and Prospecting, China University of Petroleum, 102249, Beijing, China.
[2] SINOPEC Southwest Oil Company, 610016, Chengdu, China.
** lindachen@cup.edu.cn*

ABSTRACT

A recent exploration verified a significant gas potential of tight sands of the Upper Triassic Xujiahe Formation from the western Sichuan basin of southwest China. The mechanism for gas entrapment in basin-centered areas needs to be further studied, and porosity evolution is a key factor for understanding this issue. In order to assess the porosity evolution in those sands, an integrated approach was applied consisting of: plane-light and ultra-violet fluorescence petrography, fluid inclusion microthermometry and properties, scanning electron microscopy, X-ray diffractometry, basic sandstone texture and mineralogical compositions, diagenetic features, pore types, and porosity and permeability. An overall diagenetic history of the Xu2 Member of Xujiahe Formation was deduced based on petrographic textural relationships, diagenetic minerals, fluid inclusion homogenization temperatures, organic matter maturation and burial history curve. Further, we constructed a porosity prediction model for the evolution history of the Xu2 Member tight gas sand after considering the initial porosity prediction model, the role of compaction and cementation on porosity loss, and the impact of dissolution on secondary porosity. The study revealed that the diagenetic process of the Xu2 Member tight sand occurred in five phases. Up to the late depositional age of the Xu4 Member, mechanical compaction was the principal factor for the loss of porosity during the Eogenesis A phase, which decreased the initial porosity by 10–12%. During the Eogenesis B phase (up to the Late Triassic), mechanical compaction, early quartz growth and carbonate cements generally caused the porosity to decrease by 6–7%. The phases Mesogenesis A and B, which lasted up to the middle Cretaceous, were the key stages for porosity loss because of the intensive compaction, cementation and formation of authigenic minerals. At the end of Mesogenesis, the remaining porosity in the tight gas sand of the Xu2 Member decreased by 6–10%. From the late Cretaceous to the present, the remaining porosity sharply decreased, and the tight sand was totally consolidated. The stimulating results show that the time of densification of the tight gas sand would have varied in the different gas fields, but the main stage of sandstone consolidation can be placed in the Middle Jurassic to the Late Jurassic.

Key words: tight gas sand; reservoir quality; sandstone diagenesis; porosity evolution; west Sichuan basin; China.

RESUMEN

Una exploración reciente verificó un significativo potencial gasífero en las arenas compactas de la Formación Xujiahe del Triásico Superior en la parte occidental de la cuenca de Sichuan del suroeste de China. Los mecanismos de entrampamiento de gas en áreas de cuenca requieren ser estudiados con mayor detalle y la evolución de la porosidad es un factor clave para entender este problema. Con el fin de evaluar la evolución de la porosidad en esas arenas, se aplicó un enfoque integral que consistió en: petrografía con nícoles paralelos y fluorescencia ultravioleta, microtermometría y propiedades de inclusiones fluidas, microscopía electrónica de barrido, difractometría de rayos X, textura y composición mineralógica básica de las areniscas, rasgos diagenéticos, tipos de poros, y porosidad y permeabilidad. Se dedujo una historia diagenética general del Miembro Xu2 de la Formación Xujiahe a partir de las relaciones petrográficas texturales, los minerales diagenéticos, las temperaturas de homogeneización de inclusiones fluidas, la maduración de la materia orgánica y la curva de la historia de sepultamiento. Además, construimos un modelo de predicción de la porosidad para la historia evolutiva de las arenas compactas gasíferas del Miembro Xu2, para lo cual se consideró el modelo inicial de predicción de la porosidad, el papel de la compactación y cementación en la pérdida de porosidad, y el impacto de la disolución en la porosidad secundaria. El estudio reveló que el proceso diagenético de las arenas compactas del Miembro Xu2 ocurrió en cinco fases. Hasta finales de la edad de depósito del Miembro Xu4, la compactación mecánica fue el factor principal para la pérdida de porosidad durante la fase de Eogénesis A, la cual desminuyó la porosidad inicial en un 10–12%. Durante la fase de Eogénesis B (hasta el Triásico Tardío), la compactación mecánica, el crecimiento temprano de cuarzo y los cementos carbonatados generalmente causaron una disminución de la porosidad en 6–7%. Las fases Mesogénesis A y B, que se prolongaron hasta el Cretácico medio, fueron etapas clave para la pérdida de porosidad debido a la compactación intensiva, la cementación y formación de minerales autigénicos. Al final de la Mesogénesis, la porosidad restante en las arenas compactas gasíferas del Miembro Xu2 disminuyó en un 6–10%. Desde finales del Cretácico hasta la actualidad, la porosidad restante disminuyó pronunciadamente, y las arenas compactas se consolidaron totalmente. Los resultados muestran que el tiempo al que ocurrió la densificación de las arenas compactas gasíferas podría haber variado en

Chen, D., Pang, X., Xiong, L., Wang, L., Xie, M., 2014, Porosity evolution in the tight gas sands of the Upper Triassic Xujiahe Formation, western Sichuan basin, China: Revista Mexicana de Ciencias Geológicas, v. 31, núm. 3, p. 361-375.

los diferentes campos de gas, pero la etapa principal de la consolidación de la arenisca habría ocurrido en el Jurásico Medio a Jurásico Tardío.

Palabras clave: arenas compactas gasíferas; calidad de reservorio; diagénesis; areniscas; evolución de la porosidad; cuenca de Schihuan; China.

INTRODUCTION

Since Masters (1979) developed the concept of deep-basin gas traps, a large number of gas accumulations have been discovered in basin-centered areas (Law, 2002), which are generally tight gas systems. In 2009, the world annual production of tight gas amounted to 15.3 TCF and one-third of the U.S. gas production for the year was from tight gas (BP World Energy Statistics, 2009). Tight gas reservoir resources in China have been discovered in a number of basins including the Ordos, Sichuan, Tuha, Songliao and Tarim basins, with a total area of 600,000 km^2 and a resource reserve of over 777 TCF (Zou *et al.*, 2012). At the end of 2010, the reserves and annual production of tight gas in China accounted for 39.2% and 24.6% of the total natural gas, respectively, and the proportions are expected to increase (Dai *et al.*, 2012). A great gas potential has been documented in tight sands of the Upper Triassic in the western Sichuan basin (Song and Hong, 2001; Zou *et al.*, 2009). The volume of recoverable gas reserves in the Xujiahe Formation was estimated at 560 billion cubic feet by the SINOPEC Southwest Oil Company in 2009. Tight gas reservoirs are defined as gas-bearing rocks with an *in-situ* porosity and permeability to gas of less than 12% and 1 millidarcy, respectively (Surdam *et al.*, 1997). The controls on porosity of tight gas reservoirs have been investigated by many geologists including Robinson and Shanley (2004) and Dutton and Robert (2010). Depositional facies and their diagenetic evolution are the main controls on sandstone reservoir quality (Johnson and Fisher, 1998; Lander and Walderhaug, 1999; Dutton and Robert, 2010). Because gas entrapment is a long geological process, the present porosity and permeability cannot be regarded as the same value in the geological stage of gas accumulation, so it is now vital from both a scientific and a practical standpoint to investigate the diagenesis and porosity evolution in low permeability sandstones. However, the diagenetic history, and its relationship with gas entrapment, has not been investigated in this basin-centered area. Therefore, the mechanism for gas entrapment in basin-centered areas needs to be further studied, and porosity evolution is a key factor for understanding this issue.

Although several previous researchers have documented the reservoir properties and distribution, sandstone diagenesis and types of pore space for the tight gas sand in the Upper Triassic Xujiahe Formation, west Sichuan basin, China (Tang *et al.*, 2004; Xu *et al.*, 2008; Zhu *et al.*, 2008; Lu and Liu *et al.*, 2009), few studies have analyzed the diagenetic history, gas charging history and porosity evolution. After about 40 years of natural gas exploration, the formation provides an excellent dataset for studying diagenetic and porosity evolution. The evolution of porosity in clastic units resulted from the interplay of depositional and diagenetic processes. As far as clastic sediments of tight gas sands are concerned, the first control on reservoir quality is primarily a function of the depositional properties such as the mineralogical composition, grain size, sorting and clay content. However, reservoir quality is more a function of diagenetic alterations for tight gas sand because over time this depositional porosity was lost due to the combination of compaction and cementation, or the porosity was increased by dissolution.

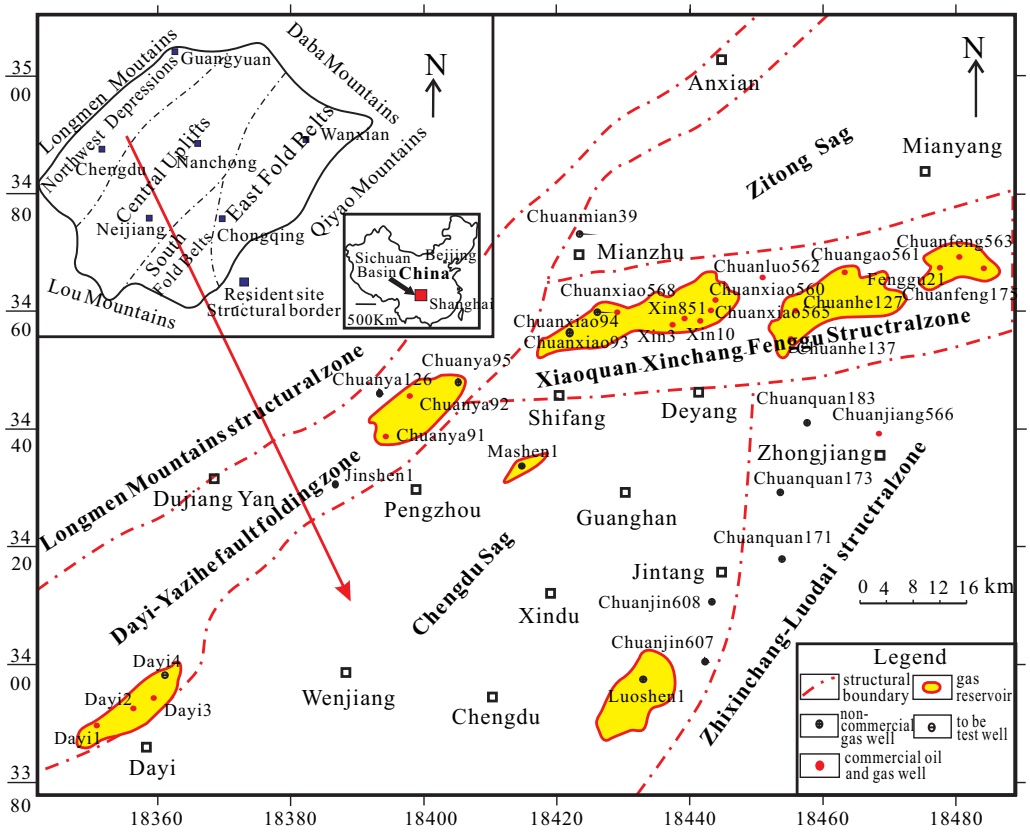

Figura 1. Location map of the western Sichuan basin, China, showing the structural elements, important gas reservoirs, and the location of sampled wells.

GEOLOGICAL SETTING

Covering an area of 230,000 km^2 with the shape of an irregular rhombus, the Sichuan basin is a multiple-cycle sedimentary basin in southwest China. The tectonic evolution of the basin can be divided into an early cratonic depression formed during Paleozoic - Early Triassic time, and a later foreland basin stage since the Late Triassic. Structurally, the basin consists of four first-order units: West Depression, Central Uplifts, and East and South Fold Belts (Figure 1). With an area of 10,570 km^2, the central part of western Sichuan foreland basin can be divided into two sags named Chengdu sag and Zitong sag and four folded structures known as Former North Longmenshan, Anxian–Yazihe–Dayi, Xinchang–Fenggu and Zhixinchang-Luodai, which make it a favorable area for gas prospecting (Figure 1). Five large gas fields are found in the upper Paleozoic tight gas sand: Xinchang, Fenggu, Dayi, Luodai and Yazihe. The early Indosinian Orogeny in the Late Triassic caused the whole Sichuan basin to be uplifted and eroded, and the western Sichuan foreland basin has developed since Late Triassic. The strata that developed from the Triassic to the Tertiary are very thick, with a maximum thickness up to 6000 meters. Gas production in the region are from the following stratigraphic horizons: Triassic Xujiahe Formation (T_3X), Middle Jurassic Shaximiao Formation (J_2s), Upper Jurassic Penglaizhen (J_3p) and Suining Formations (J_3sn) (Figure 2). Source rocks are mainly distributed in the Upper Triassic Xujiahe Formation (T_3X) terrestrial coal measures and Lower Jurassic lacustrine mudstone.

The strata of the Upper Triassic Xujiahe Formation contain five members named from bottom to top: T_3m-T_3t, T_3X^2, T_3X^3, T_3X^4 and T_3X^5. First, T_{3m}-T_3t is dominated by continental shelf black shale and mudstone. The second member (T_3X^2, abbreviated Xu2) is a thick-bedded grayish arkosic arenite and lithic arenite, developed in a deltaic environment (Figure 3). Next, T_3X^3 is dominated by black mudstone interbedded with coal beds, formed in a shallow lake setting. Dark mudstone and interbedded coal seams are the main source rocks. The cumulative thickness of the coals is generally greater than 10 meters, with the maximum up to 35 meters. Fourth, T_3X^4 developed grayish fine-to-medium grained calciferous lithic arenite, with variegated conglomerate, with dark gray muddy siltstone and coal seams interbedded. The sandstones are generally deposits from deltaic plains, delta fronts in the center of the basin, and fan deltas close to the boundaries of the basin. The fifth member, T_3X^5, was also formed in a shallow lake setting, dominated by black shale and dark gray muddy siltstone interbedded with dark gray, fine-to-medium grained muddy calciferous litharenite. In the lower part of the T_3X^5, the shale and muddy siltstone have coal seams interbedded. In the present study, the Xu2 Member, with an average porosity generally less than 4%, was selected for the study of the porosity evolution because this section of the formation has extremely low porosity and permeability compared to other reservoirs in the Xujiahe Formation.

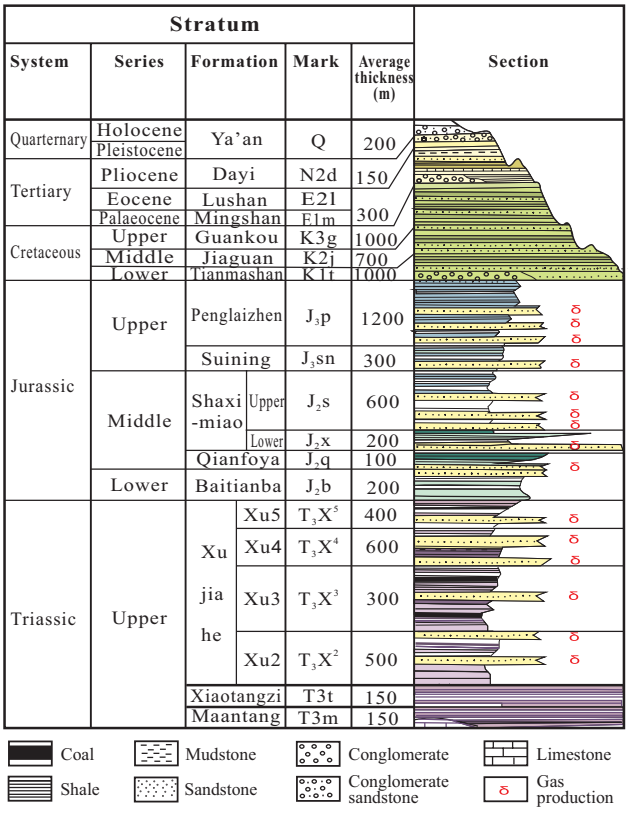

Figura 2. Generalized stratigraphy of the western Sichuan foreland basin.

MATERIAL AND ANALYTICAL METHODS

Porosity and permeability of 316 representative sandstone samples from cores of 35 wells were measured. These samples include the differ-

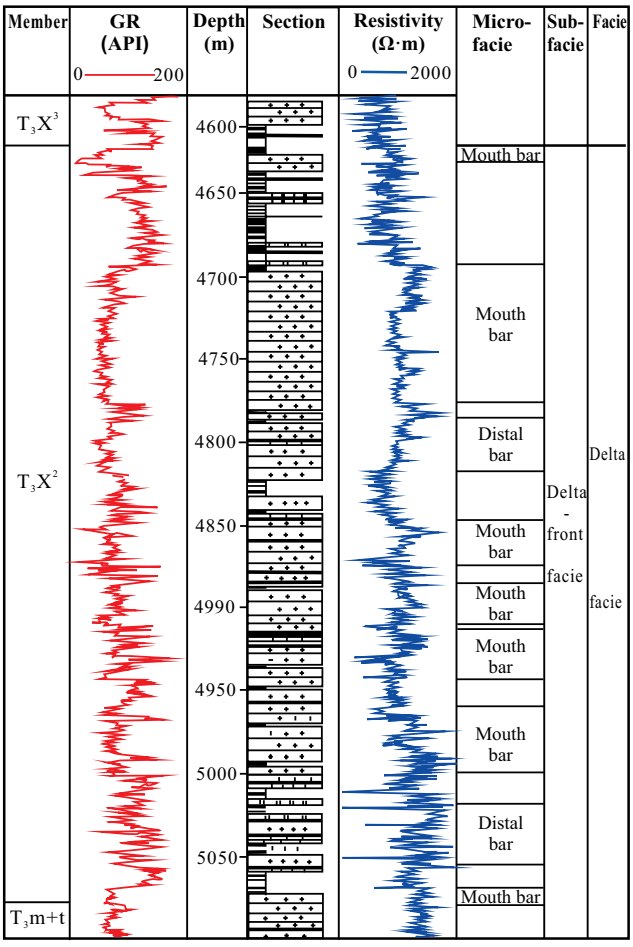

Figura 3. Lithology column of well Xin853, showing the microfacies of the deltaic environment in the Xu2 sandstones. GR: gamma radiation.

ent facies of the Xu2Member and cover the range of present-day burial depths. Those analyses were not performed directly for this work and 168 samples from 16 wells were taken for this manuscript and used in thin-section petrography, ultraviolet fluorescence microscopy, fluid inclusion microthermometry, scanning electron microscopy (SEM) and X-ray diffraction (XRD) measured by the Chinese State Laboratory of Petroleum Resource and Prospecting, as described later (sample location shown in Figure 1). To reveal the diagenetic and porosity history of the main reservoir sandstones in the Xu2 Member, core samples were selected from wells at different localities of the West Sichuan Basin China (WSDC,) including the deep sag, fold structures and slope areas. Some data from the central uplift of the Sichuan basin were also utilized in this work because of their shallower burial depth. Sandstone samples in the Xu2 Member were also selected from each well at a sampling depth interval as evenly as possibly. The sample depths ranged from approximately 2000 to 5500 meters and include sandstones of varying porosity and permeability.

Thin-section petrography was used to determine mineral composition, diagenetic relationships, porosity characteristics, and clay growth occurrence and habits in the pore space. The samples for thin-section petrographic studies were impregnated with blue epoxy to facilitate the recognition of porosity. Quantification of the mineralogy and thin-section porosity was achieved by counting a total of 200 points per thin section. Diagenetic features and crosscutting relationships were examined using conventional thin-section petrography. The staining method of Dickson (1965) was used to further identify the carbonates. Ultraviolet fluorescence petrography was carried out on a Leica DMLP microscope to identify bitumen, oil and gas inclusions. Other inclusions were also identified using the same microscope. Homogenization temperatures of fluid inclusions were measured with a Linkam Heating/Freezing stage of type THMS600, with a precision better than 0.1 °C.

Scanning electron microscopy (SEM) was employed to characterize authigenic clays, intergranular cement, and feldspar alteration. An Oxford LEO-435VP scanning electron microscope equipped with an Oxford energy dispersive X-ray spectrometer was used to observe the cement morphology, pore geometry and diagenetic relationships. The accelerating voltage was 20 kV with a current emission of 50–100 pA.

The mineralogical composition of clays was determined by X-ray diffraction (XRD) using a Rigaku D/max 2550 X-ray diffractometer with Cu Kα radiation operated at 100 mA and 40 kV. Clay sub-samples (<2 mm) were prepared in accordance with the guidelines of Moore and Reynolds (1997). Calcium carbonate was removed from samples with an acetic acid–sodium acetate buffer, with the pH being adjusted to 5 prior to clay separation by centrifugation. Clay minerals were identified according to the position of the (00l) series of basal reflections on XRD patterns of air-dried, ethylene-glycolated (at 60 °C for 7h), and heated specimens (at 550 °C for 2.5h). Peak areas of clay minerals were employed for the semi-quantitative determination of the clay mineral content.

RESULTS

Petrologic features

Most tight gas sand samples of the Xu2 in the study area are fine (0.1–0.25 mm) to medium (0.25–0.5 mm) grained, thick-bedded grayish sand. Litharenite, sublitharenite and sub-arkosic sandstone are the major components of the tight sand. The sand also partly consists of arkose, feldspathic litharenite and quartzarenite. Point counting data show that the most common detrital grains are quartz (~60–80% of rock volume, mean 70.4%), K-feldspar and plagioclase (mean 8.6%), and lithic fragments (~10–30%, mean 21%). Quartzite chert, slate, and schist, dominate the lithic grains, with mudstone fragments also present. The remaining is comprised of a clay matrix and cements of quartz, authigenic kaolinite, calcite, dolomite and siderite. The interstitial matter comprises clay matrix and cement, with an average of 7.2% of rock volume. The matrix is composed of clays and quartz grains of fine silt size, and averages 1% of volume, and cement makes an average of 6.2% of rock volume. In a few cases, clayey patches may represent a pseudomatrix derived from the deformation of sand-sized clay aggregates. The sandstones are moderate to well sorted. Silty and sandy grains are rounded to sub-rounded but typically non-equant. Based on angularity, sorting, and matrix content, most of sandstones are of medium mineralogical maturity.

Diagenetic features

The mineralogy and petrophysical properties of sandstones from the Xujiahe Formation in the western depression of Sichuan basin have undergone significant diagenetic modification. The diagenetic processes that have affected the reservoir quality of the tight sandstones include mechanical and chemical compaction, precipitation of quartz, ankerite, Fe-calcite, calcite, chlorite, illite, albite and K-feldspar, dissolution of unstable mineral grains such as feldspar, carbonates and chlorite, and fracturing.

Mechanical and chemical compaction

The sandstones display considerable compaction effects. Brittle quartz and feldspar grains have been intensively fractured (Figure 4a). The mechanical fractures have been regarded as the results of rapid, deep burial (Chuhan *et al.*, 2002; Makowitz *et al.*, 2006). The western Sichuan basin has undergone intensive structural subsidence because the adjacent Longmen Mountains were uplifted in the late Triassic, affected by the orogeny of the Tethys Sea (Wang, 2001). Ductile clay- and silt-rich rock fragments and micas were bent around resistant detrital grains (Figure 4b, 4c). Ductile mud clasts have locally been deformed sufficiently to produce a pseudomatrix, thus decreasing porosity. Additionally, grain contacts are predominantly concave-convex, with subordinate suturing contacts and rare point contacts (Figure 4d). Suturing contacts generally indicate some degree of intergranular pressure solution.

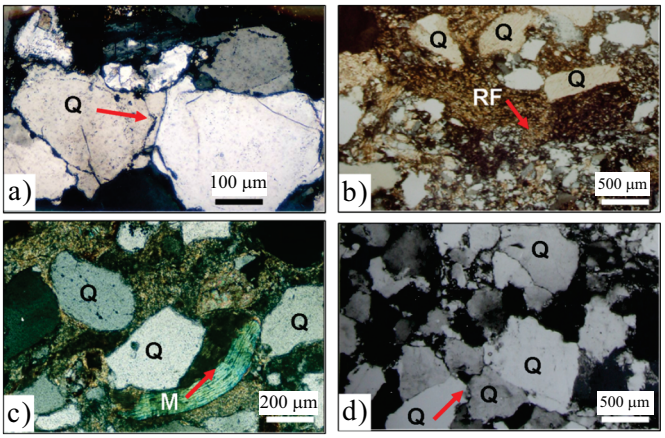

Figura 4. Photomicrographs of mechanical and chemical compaction with arrows showing the features. (a) Fracturing of brittle grains in the sandstone of well Xin853 at 3408.48 m. (b) Rock fragments and micas bent around resistant detrital grains in the sandstone of well Chuanya92 at 2796.5 m and (c) in the sandstone of well Xin853 at 3397.25 m. (d) Concave-convex grain contacts and fractures in the sandstone of well Chuanmian93 at 4056.0m. Q=quartz, RF=rock fragments, M=mica.

Cementation

Calcium carbonate and quartz are the volumetrically most significant cements in the sandstones of the Xujiahe Formation in the WSDC. Minor cements include illite, chlorite, kaolinite, dolomite and siderite. Authigenic feldspar and evaporitic minerals are generally absent in the Xujiahe Formation.

Clay cement developed widely in the sandstone. Diagenetic clay minerals constitute 7.6% of cements on average and were distinguished from the detrital matrix by their presence as distinctive pore fills and within altered minerals. These clays have a predominately illitic composition. Authigenic hair-like, pin-like and concentrated as pendular aggregates, illite occurs in many samples with an abundance exceeding 4% of rock volume. Illite grows into pore space engulfing calcite and quartz. Some chlorite is easily discerned occurring as detrital intraclasts. Clay coats on framework grains (Figure 5a) were also identified, which are locally concentrated as pendular aggregates attached to the lower surface of grains. Kaolinite is often booklets-like or worm-like and fills the secondary solution pore space of feldspar.

Quartz cements are also common throughout the Xujiahe Formations. Quartz constitutes 13% of cement volume on average. As the predominant form of quartz cement in the tight sandstones, syntaxial overgrowths are easily distinguished from the detrital host by the occurrence of clay rims. They represent an important porosity-reducing mechanism relative to the burial history. Less abundant are veins of microcrystalline quartz with some euhedral and subhedral crystals. Although difficult to image, some silica cement is probably associated with pressure solution at grain contacts. Authigenic quartz occurs as 0.05~0.3 mm wide overgrowths on detrital quartz grains, occupying between 2 and 12% of rock volume (with an average of 8%). Authigenic quartz also occurs as outgrowths up to 40 μm long, especially on chlorite coated quartz grains. Up to three phases of quartz overgrowth can be recognized with dust lines between them (Figure 5b), which illustrates discontinuous overgrowth. In Figure 5b, the quartz overgrowth (stage I, blue arrow) on the quartz grains grew mainly towards the rim of the grains, was overlain by the quartz overgrowth of the second phase (stage II, green arrow), which grew toward the lower. The latter was in turn overlain by the third phase (stage III, red arrow).

Carbonate minerals are among the most dominant cements by volume, 80% on average. Geochemical analysis of the carbonate has identified calcite, dolomite, siderite, ankerite, and ferroan calcite. The carbonate cements are generally distributed as intergranular, pore-filling crystals. The crystals vary from microcrystalline to coarsely crystalline and locally poikilotopic mosaics. Two stages of calcite cementation appear to be ubiquitous in samples under cathodoluminescence (CL) (Figure 5c, 5d): stage I is of orange-yellow luminescence with or without relatively dull zones presenting calcite, locally zoned, whereas stage II is characterized by non-luminescent or very dull ferroan calcite. Volumetrically, stage II is much more dominant than stage I. Stage I carbonate cements are dominated by calcite. In calcite-cemented sandstones, except for minor muddy infills, there is no quartz overgrowth (Figure 5c). This phenomenon suggests that calcite cements were formed before the main compaction stage. In some samples, feldspars were dissolved but no calcite filled in pores formed by feldspar dissolution. This may indicate that the calcite cements were formed before feldspar dissolution. Textural relationships for both pore-filling cements and replacements, including grains that appear to "float" within poikilotopic cements, also indicate that the cementation took place during early burial, when the cements had experienced only a slight degree of compaction. Early carbonate cements, primarily of non-ferroan calcite, occur as poikilotopic crystals with coarse euhedral crystal texture and less frequently as mosaics of rhombic crystals dispersed among the framework grains. These coarse-grained calcites are pore filling with dimensions of 10–300 μm. Secondary pores associated with feldspar and lithic grain dissolution are commonly filled with Phase II carbonate cement (Figure 5d), but not with Phase I dolomite, suggesting that Phase I calcite was developed prior to significant dissolution of feldspar and lithic grains. Phase II carbonate cements are predominantly dolomite, ankerite and ferroan calcite. Dolomites usually appear as rhombus crystals overprinting early carbonate cements. It may suggest that they formed during deeper burial through local Mg concentration from internal sources (dissolution of clasts and earlier cements). Less than 2% of patchy ferroan calcite cements typically fill intergranular and dissolution pores. The ferroan dolomites (ankerite) commonly have a lower percentage in rocks (<1%) and also appear as rhombus crystals. Ferroan calcite and ankerite are by far the most abundant late diagenetic minerals in the tight gas sands with a burial depth. They show a wide range of textural and compositional varieties and reflect important genetic differences. Ankerite cement occurs, in general, as euhedral, fine- and medium-sized crystals, with crystal size increasing with depth. In some samples, pores are completely occluded by late-stage ferroan calcite and ankerite. Detrital grains appear to float in calcite cement.

Dissolution

Dissolution is widespread in the studied tight sandstones and was identified from the early to late diagenesis by the investigation of blue or red epoxy thin sections and SEM. Detrital feldspar, carbonate and volcanic rock fragments, and rarely quartz, show evidence of dissolution (Figure 6). Intergranular and intragranular, as well as moldic pores, can be found in the thin sections. Secondary intragranular pores have been developed by the partial to pervasive dissolution of plagioclase, volcanic rock fragments and mud intraclasts. Moldic pores have been formed; presumably they were occupied by plagioclase crystals. The plagioclase grains are dissolved, being frequently associated to the formation of kaolinite (Figure 6). The dissolution of plagioclase grains is also commonly associated with variable degrees of albitization. Two

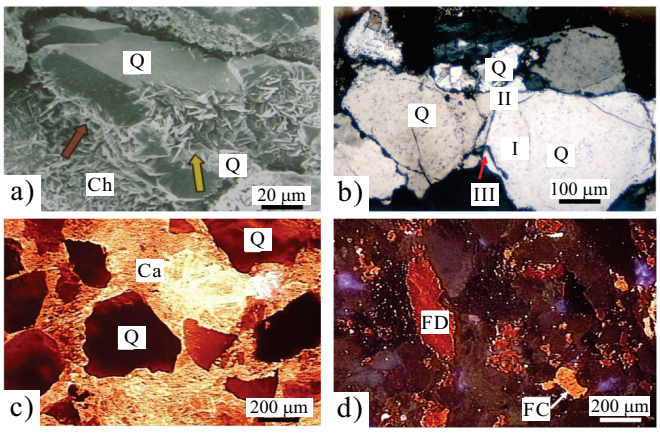

Figura 5. Photomicrographs of cementation. (a) SEM image showing chlorite developed along the boundary of quartz grains (yellow arrow) and quartz cement (red arrow) in the sandstone of well Chuangao561 at 4993.29 m. (b) Optical micrograph showing three stages of quartz growth (I, II, III) with dust lines between them in the sandstone of well Chuanxiao560 at 4812.42 m. (c) Cathodoluminescence (CL) image of early stage non-ferroan calcite showing orange-yellow luminescence in the sandstone of well Dayi3 at 4685.2 m; (d) CL image of late stage ferroan calcite and dolomite showing dull luminescence in the sandstone of well Dayi3 at 3997.13 m. Q=quartz, Ch=chlorite, Ca=calcite, FD=ferroan dolomite, FC=ferroan calcite.

dissolution textures are seen in the thin sections. The first is dissolution along cleavages and fractures in feldspar, rock fragments and, rarely, quartz. The second is grain-contact dissolution of quartz and local plagioclase through pressure solution. Carbonate cement and local carbonate grains were dissolved in places. The phenomenon of carbonate cement-filled pores seems to indicate the total dissolution of framework grains and also that the dissolution took place earlier than the late-stage carbonate cementation.

Fracturing

Small fractures can be seen in the thin-section images of some quartz and feldspar grains (Figure 4a, 4b). They can be interpreted to have originated from above by compaction, and filled locally with microcrystalline quartz, clay and carbonates during diagenesis. These small fractures range in width from 0.01–0.02 mm. Larger open fractures can also be observed in thin sections including fracture systems sub-parallel to the bedding and prominent fractures in feldspar, quartz and rock fragments (Figure 7c, 7d). Vertical fractures, horizontal fractures and reticular fractures are found in core samples (Figure 7a, 7b). Some large fractures were filled with microcrystalline quartz, larger quartz crystals (Figure 7b), calcite and siderite. In some samples, fractures are the major pore space in the reservoir. These large fractures usually range in width from 0.5 to 5 mm. Fractures and joints are prominent in a variety of scales at megascopic scale. Also present are numerous veins of quartz and local calcite (Figure 7b). The structural geology shows that the western Sichuan basin has undergone intensive deformation since the Late Triassic. The Indosinian (Late Triassic), Yanshan (Jurassic to Cretaceous) and Himalayan movements (Tertiary to Quaternary) brought about intensive structural fractures in the tight sand (Yang, 2003). The investigation of well cores shows that the fractures have high linear density characteristics; that is, they show from 20 to more than 60 fractures per meter in core space (Table 1).

Pore types and porosity

Types of reservoir pores in the tight sandstones are of primary and secondary origin. Though the distinction between intergranular pores of primary and secondary origin is problematic, it is necessary to determine the value and relative abundance of different pore types – primary and secondary pores, and micropores – to fully understand the processes involved in porosity loss and increase and to estimate reservoir quality. Based on both plane-light petrography and SEM, three genetic pore types were identified: remaining intergranular pores, secondary dissolution pores, and fractures. They constitute a total volume of pore space of 21%, 74% and 5%, respectively. The remaining intergranular pores originated from the remains of primary intergranular pores after diagenetic alteration, like compaction and cementation. The remaining pores are usually small and show different types, including unequal polygons, triangles and rhombuses. When intensive compaction affected the reservoir, the remaining pores would usually present strip-like or linear shapes (Figure 8a). The boundary of the remaining intergranular pores often developed with a thin chlorite film and was usually partly filled by authigenic quartz or calcite. The volume of remaining intergranular pores makes up a minority of rock volume, less than 1%, and has patchy distribution in the core samples.

Secondary dissolution pores include pore space within a dissolved framework of grains and oversized pores that formed by partial-to-complete grain dissolution. Most dissolution pores in the Xujiahe Formation tight sands formed by the dissolution of K-feldspar. Partial dissolution pores originated from quartz cement, mica, and calcite. In contrast to remaining primary intergranular pores, the secondary dissolution pores make up more of the rock volume, ranging from 1-6%, 3% on average. In some samples (Figure 8b, 8c), it was seen that the dissolution pores of K-feldspar were partly filled by late-stage authigenic ankerite, which indicates that the dissolution process occurred earlier than the phase II carbonate cementation. Authigenic kaolinite, illite and quartz also precipitated and partially filled the secondary dissolution pores of K-feldspar.

Micropores were defined as pores having pore-throat radii of 0.5 μm or less. Although it is difficult to quantify the microporosity accurately in thin sections, it is the third important pore type in the tight sand. The capillary-pressure data can be used to estimate the volume of microporosity. Micropores can be primary or secondary, and they

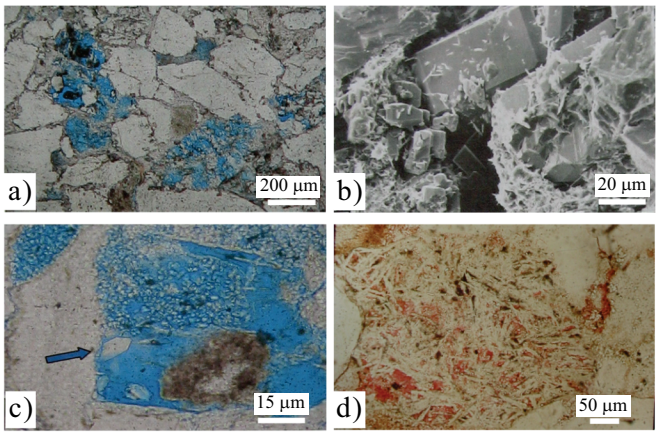

Figura 6. Photomicrographs of dissolution. (a) Blue epoxy thin-section image of K-feldspar dissolution in the sandstone of well Chuangao561 at 4931.2 m; (b) SEM image showing the dolomite crystal infill of the dissolution pore space of feldspar in the sandstone of well Chuangao561 at 3712.2 m; (c) Blue epoxy thin-section image indicating authigenic kaolinite and quartz growth (blue arrow) in the pore space of K-feldspar dissolution in the sandstone of well Chuanxiao565 at 3549.53 m; (d) Red epoxy thin-section image of dissolution of rock fragments in the sandstone of well Chuanya92 at 2793.48 m.

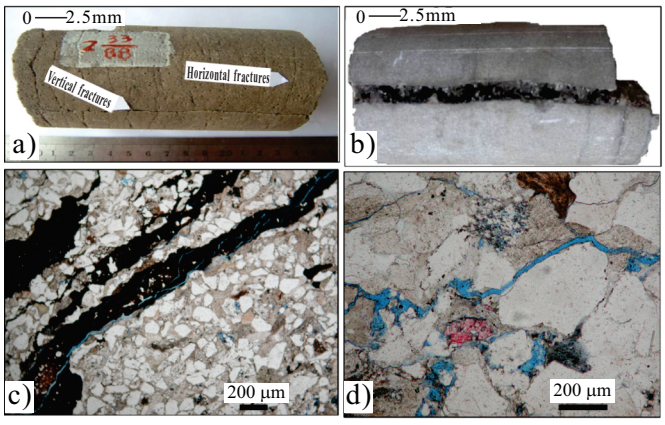

Figura 7. Photos and micrographs of cores showing fractures developed in the Xu2 member tight sand. (a) Core fragment showing vertical and horizontal fractures in the sandstone of well Xin10 at 4883.05–4883.17 m. (b) Core showing infilling of a vertical fracture by veins of quartz in the sandstone of well Chuanxiao565 at 5058.66–5062.69 m. (c) Micrograph showimg organic matter infilling in microfractures sub-parallel to the bedding in the sandstone of well Chuangao561at 3695.41 m. (d) Micrograph of fractures passing through quartz grains in the sandstone of well Chuangao561at 3701.3 m.

Table 1. Distribution of fracture properties in sandstone samples from cores of the Xu2 Member.

Well	Depth of the core (m)	Length of the core (m)	Number of fractures	Density (number/m)
Xin3	4731.06–4731.53	0.47	3	6.38
Xin3	4928.52–4930.82	2.30	2	0.87
Xin3	4932.90–4932.92	0.02	1	50
Xin10	4847.45–4849.81	2.36	32	9.52
Xin10	4850.50–4855.91	5.41	69	12.75
Xin10	4880.15–4888.15	8.00	251	31.38
Xin10	4925.64–4927.95	2.31	42	18.18
Chaunxiao560	4804.01–4805.81	1.80	28	15.56
Chaunxiao560	4924.25–4926.00	1.75	115	65.71
Chaunxiao565	5058.65–5060.16	1.50	41	27.33
Chaunxiao565	5069.21–5071.34	2.13	59	27.70

usually occur in matrix, authigenic clays or altered grains. The kaolinite intercrystalline pores can be identified in some samples by investigation of red epoxy thin section (Figure 8d).

The porosity and permeability are important petrophysical features of sandstone reservoirs. The statistics of their features are closely associated with the reservoir quality. In this study, the porosity and permeability were measured for core plugs (3.8 cm in diameter) using a nitrogen permeameter within a confining chamber loaded up to 10,000 psi. The nitrogen porosity and permeability of each sample were measured at a confining pressure of 100 and 400 psi, respectively. The sandstones of the second member of the Xujiahe Formation are tough and compact. The average porosity of core plugs from 270 core samples of ten wells is 3.4%, with a range from l to 6.5% (Figure 9a). The porosity distribution features show that most reservoirs have porosity ranging from 3–4%. Less than 10% of samples have porosity higher than 5%. These values match well with two-dimensional estimates from thin sections, which average 2.8%. A few porosity estimates from thin sections were as high as 9.69%, and inspection shows that these more porous samples are either highly fractured or contain abundant partially dissolved feldspar. Permeability of the 270 samples averages 0.045 mD, with a maximum value exceeding 100 mD (Figure 9b). The permeability distribution features shows that permeability in most reservoirs ranges from 0.05 to 0.1 mD. Less than 10% of the samples have permeability higher than 0.1 mD. A cross-plot of porosity versus permeability exhibits a positive relation only if the sandstones have a permeability less than 1mD (Figure 9c). This positive relation is challenged when the permeability of sandstones is higher than 1 mD, with the possible reason being that the fractures enlarged the permeability of core samples. Here, the porosity and permeability of the samples are extremely low because the reservoirs are in the tight sandstones.

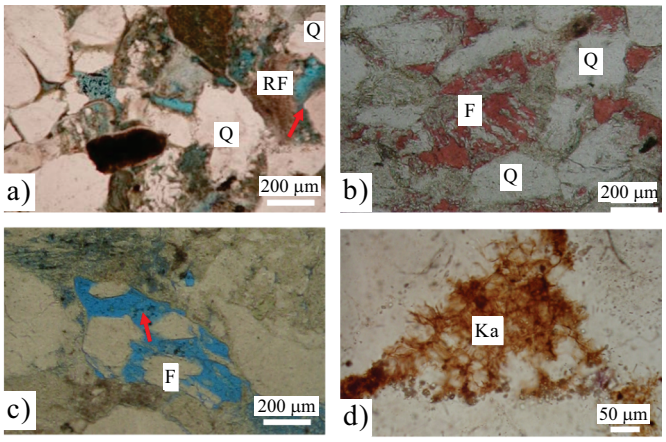

Figura 8. Optical micrographs of pores types. (a) Blue epoxy thin section image of strip-like or linear shaped remaining intergranular pore (arrow) in the sandstone of well Dayi4 at 4962.48 m. (b) Red epoxy thin-section image of dissolution intergranular pores and intragranular pores of feldspar in the sandstone of well Chuangao561 at 3549 m. (c) Blue epoxy image of dissolution intragranular pores of feldspar in the sandstone of well Chuanxiao565 at 3560 m. (d) Red epoxy image showing kaolinite intercrystalline pores in the sandstone of well Chuanmiao39 at 4051.0 m. Q=quartz, RF=rock fragments, F=feldspar, Ka=kaolinite.

Fluid inclusions

A fluid inclusion microthermometry study was performed on 64 samples from ten wells (location shown in Figure 1). Aqueous inclusions occur in the cement overgrowths as isolated inclusions, in groups or in trails, which occasionally cut into the detrital part of the grain (Figure 10a, 10b). Both ferroan and non-ferroan calcite cement horizons (including the poikilotopic calcite fracture) contain abundant aqueous inclusions (Figure 10c). The inclusions occur in groups or as isolated inclusions, and they are interpreted to be primary. Aqueous

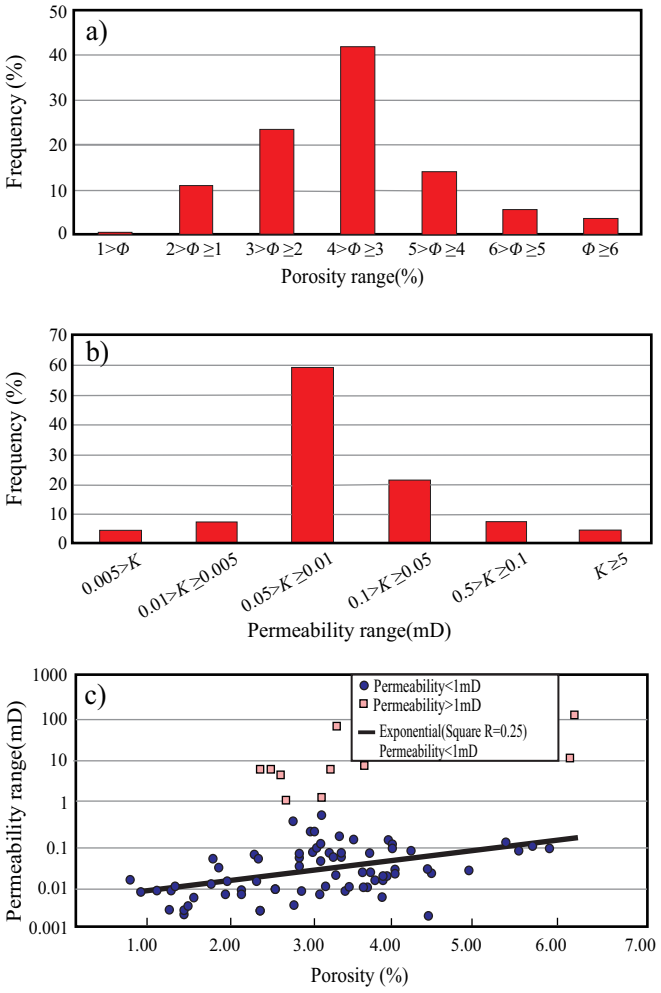

Figura 9. (a) Porosity and (b) permeability distribution histogram, (c) a cross plot of porosity versus permeability of the Xu2 tight gas sand.

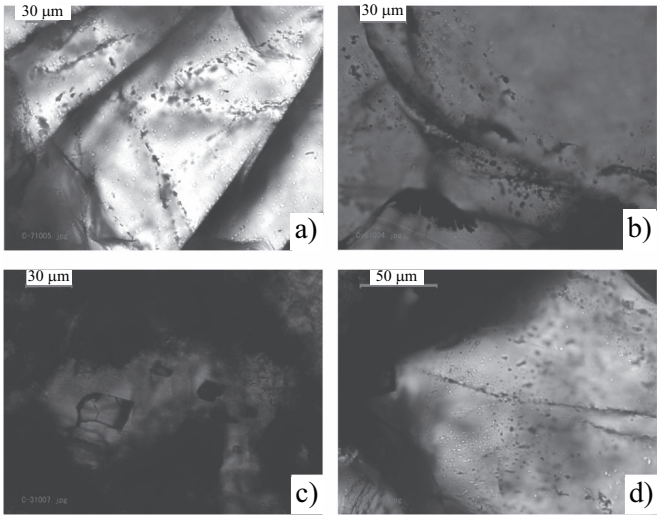

Figura 10. Optical micrographs showing the fluid inclusion developed in the Xu2 member tight sand. (a) Micrographs showing liquid hydrocarbon inclusion encircling the quartz growth in the sandstone of well Dayi3 at 4689.3 m, and (b) in the sandstone of well Chuaoxiao94at 3827.6 m. (c) (d) Micrographs of calcite cement horizons containing abundant aqueous inclusions in the sandstone of well Chuanfeng125 at 44789.5 m. Aqueous inclusions developed in fractures, which pass through the quartz growth in the sandstone of well Chuanya95 at 4156.9 m.

inclusions have been also found in fractures containing both very coarse-grained, transparent calcite and "dusty" calcite. The inclusions occur isolated, in groups or in trails, and in a high proportion of all the samples (Figure 10d). Most inclusions have gas-to-liquid ratios of less than 15%, without fluorescence. The abundance of petroleum inclusions in the fractures is relatively high. Oil and gas inclusions with fluorescence shown were also found and indicate oil and gas charging in the reservoirs. The fluid inclusions are mostly 3–10 μm in size, but range up to 25 μm. The salinities range from 2.0–22.98 wt.% NaCl equiv. Salinities display a bimodal distribution with one population between 2.0–9.0 wt.% NaCl equiv, and the other between 19.0 – 22.98 wt.% NaCl equiv.

Homogenization temperatures of fluid inclusion are shown in Table 2. Different forms of authigenic quartz, including growth quartz and quartz cementation in the dissolution pores or remaining intergranular pores yielded homogenization temperatures that range widely from 63 °C to 199.5 °C, indicating a long-term diagenesis and a multiple-stage occurrence. The homogenization temperature of fluid inclusions in calcite cement differs greatly. Non-ferroan calcite has a lower homogenization temperature, less than 105 °C, and the lower homogenization temperature of ferroan calcite and dolomite is higher than 110 °C. The homogenization temperature of inclusions hosted in fracture calcite or quartz is even higher than that of other inclusions, generally being greater than 120 °C.

DISCUSSION

Diagenetic history

Burial history

We reconstructed the burial history and formation temperature evolution to make an account of the diagenesis and porosity evolution. The eroded amounts of sedimentary strata at the location of well Chuanxiao565 are 210 m in the late Triassic-Jurassic and 1780 m after the end of the early Cretaceous (Li *et al.*, 2010). The compaction coefficients (Luo and Vasseurm, 1992) of mudstone and sandstone are 0.0004 m^{-1} and 0.00025 m^{-1}, respectively. The heat flows for Triassic, Jurassic and Cretaceous times were estimated as 60, 80 and 48.5 mWm^{-2}, respectively. Additionally, a heat event occurred in the Early Cretaceous with heat flows of 81–95 mWm^{-2} (Yang and Li, 2004). Figure 11 shows the burial history of well Chuanxiao565 with the homogenization temperature data from quartz overgrowths of this well. The modeled maximum paleogeothermal gradient in the early Cretaceous is about 3.5 °C/100 m, and the gradient value during the Triassic and Jurassic is 2.6 °C/100 m, but decreases to 2.12 °C/100 m after the Late Cretaceous, coinciding with the results of Ye *et al.* (2004). Figure 11 shows the burial history of well Chuanxiao565. The modeling results show that in the Late Triassic the burial depth of the Xu2 increased sharply, to depths ranging from 2600 to 3200 m, with an average depth of 2900 m. This burial depth changed to 4880–5220 m at the end of the Late Jurassic. The maximum burial depth of the Xu2 even exceeded 6100 m during the middle Cretaceous.

Diagenetic processes

Although it is difficult to constrain the precise timing and duration of the diagenetic processes, an overall diagenetic evolution for the studied sandstones was defined on the basis of petrographic textural relationships, diagenetic minerals, fluid inclusion data, illite/smectite ratio, organic matter maturation and the burial history. Five diagenetic processes were identified for the tight sand of the Xu2 Member (Figure 12). Eogenetic alterations were controlled by several parameters such as pore-water chemistry, depositional facies, and detrital miernalogical composition. The eogenetic alterations exerted a critical control on the pattern of mesogenetic evolution and related reservoir quality modifications. According to the paleo-temperature, petrographic textural relationships, diagenetic minerals, fluid inclusion, and organic matter maturation, two eogenetic sub-processes could be constructed: Eogenesis A and Eogenesis B.

Eogenesis A occurred at burial depths below 1500 m and at temperatures of less than 65 °C. During this diagenetic stage, the organic matter had not entered the oil window yet as is suggested by the vitrinite reflectance data (VR_o %) with values lower than lower than 0.5%. In Eogenesis A, the sediments did not totally solidify to form rock, and compaction was the major diagenesis process, accompanied by early calcite cementation, grain-coating chlorite, and occasional dissolution of feldspar and rock fragments. However, the volume of cementation was very low. Grain-coating chlorite and illite prohibited the precipitation of more extensive quartz overgrowths. Measurements show that the volume of chlorite in the thin sections is 4% on average. Primary intragranular pores partially remained in this process. Based on this reason, Eogenesis A was a key stage for the decrease of porosity in the tight sand.

Eogenesis B occurred at burial depths of 1800–2500 m and at temperatures higher than 65 – 86 °C. The organic matter just entered the oil generation threshold with VR_o% reaching 0.5%. The eogenetic B alterations resulted in the growth of authigenic quartz, dissolution of feldspar and rock fragments, authigenic illite, intensive mechanical compaction and partial chemical compaction. The intensive compaction and quartz growth made the primary pores decrease greatly, however secondary pores developed because of the dissolution of feldspar and rock fragments.

Mesogenetic alterations can be also subdivided into two processes: Mesogenesis A and Mesogenesis B. Mesogenesis A process, which include the processes that occurred at burial depths greater than 2500 m, were controlled by increasing temperature (>85 °C) and by

Table 2 Homogenization temperatures and age of diagenetic minerals in sandstones of the Xu2 Member.

Well	Host mineral	Homogenization temperature (°C)	Average (°C)	Depth (m)	Age	Diagenetic sequence
Dayi2	Calcite cement	105	105	4958.6	early T_3X^4	Early calcite and dolomite cementation
Chuanya92	Dolomite cement	89	89	4859.1	early T_3X^4	
Chuanxiao93	Quartz growth	105,117,70,58,81,85,62	83	4548	late T_3X^4	Early quartz growth
Chuanhe127	Quartz growth	74,77,78,71,75,77,80,85,87,90,72	78	4584.94	late T_3X^4	
Xin851	Quartz growth	77,75,75,83,103,54,64,74	75	4796	late T_3X^4	
Chuanhe139	Quartz growth	67,72,77,75,78	74	4541	late T_3X^4	
Chuanya92	Quartz growth	64,75,66,67,80	70	4520	late T_3X^4	
Dayi2	Quartz growth	118,119,120,112,113,108,109,110,96,97,98	109	4958.6	early J1	Middle quartz growth
Dayi2	Quartz growth	68,83,72,87,78,91,108,125,171,157,11,127,176,162, 117,165	118	4579.83	early J3	
Chuanxiao560	Authigenic quartz in pores	124.5,120.3,117.6	121	4926	middle of J3	Middle-late dissolution
Chuanxiao560	Authigenic quartz in pores	125.2	125.2	4860.8	middle of K1	
Chuanhe137	Ferroan calcite cement	120,110,108,125,114,000	115	4618.4	middle of J3	Middle calcite cementation
Chuanhe127	Ferroan calcite cement	150,200,141,152,182,156,119,105,138,196	153.9	4563.3	late J3	
Chuanhe137	Quartz growth	91,88,148,93,93,154,97,97,159,101,170,180	128	4621.09	late J3	Middle quartz growth
Chuanhe127	Quartz growth	169,88,67,76,90,144,105,151,95,152,114,154,104, 162,119,180,184,200,168,186,199,197,200,201	148	4843	late J3	
Xin851	Ferroan calcite cement	171,125,135,153,147,170,117.6,135,154,161,153	147.3	4834	early K1	Late calcite cementation
Chuanxiao565	Quartz growth	199.5	199.5	5049	early K2	Late quartz growth
Chuanhe137	Calcite cement filling in fracture	121,121,138,138	129.5	4618.4	late K2	Late fracturing
Chuanya95	Calcite vein	124,132,133,121,126,127,130,131	127	4474	E3	

the types and distribution patterns of eogenetic alterations. Organic matter entered the maturation stage to generate large amounts of oil and gas with maximum VR_o% reaching 1.3%. In this processes, many diagenetic minerals were active. In addition to the compaction and quartz growth, late ferroan calcite and dolomite, which began to develop in this processes, destroyed the primary pores.

Mesogenesis B was another stage of porosity decrease in the tight sand. Despite the continued dissolution, late quartz growth and late ferroan calcite and dolomite drastically destroyed the primary pores. Moreover, the cementation and formation of authigenic minerals such as quartz and clay minerals occupied the secondary dissolution pores, which left both the intergranular and intragranular pores undeveloped. Mesogenesis B occurred at burial depths greater than 3500 m and at temperatures higher than 120 °C. The organic matter entered a highly mature stage for gas generation with a maximum VR_o% reaching 1.8%.

The last diagenesis processes for the Xu2 Member sand is the telogenesis. Telogenesis occurred at burial depths greater than 4500 m and at temperatures higher than 160 °C. The organic matter almost entered the over mature stage with VR_o% being greater than 2.0%. In this processes, only quartz growth and authigenic feldspar, with occasional chemical compaction, badly destroyed the remaining pores. Dissolution almost disappeared because of the lack of acidic fluids and organic matter. However, late structural deformations like the Yanshan Orogeny (Jurassic to Cretaceous) and Himalayan Orogeny (Tertiary to Quaternary), brought about intensive structural fracture development. In this view, of course, the fractures actually developed in the whole diagenesis.

Porosity evolution model

Many geologists have constructed different porosity prediction models. Athy (1930) defined an exponential relationship between normally pressured sediments and porosity, describing the rate at which the exponential decrease in porosity takes place with depth. Lander and Walderhaug (1999) introduced an equation based on simulating the evolution of sandstone porosity and composition through the geological history of the modeled unit. Scherer (1987) considered the controls of age, detrital quartz content, the maximum depth of burial, sorting, overpressure and median grain size on porosity for lightly cemented sandstone. For the tight gas sand of the Xu2 Member,

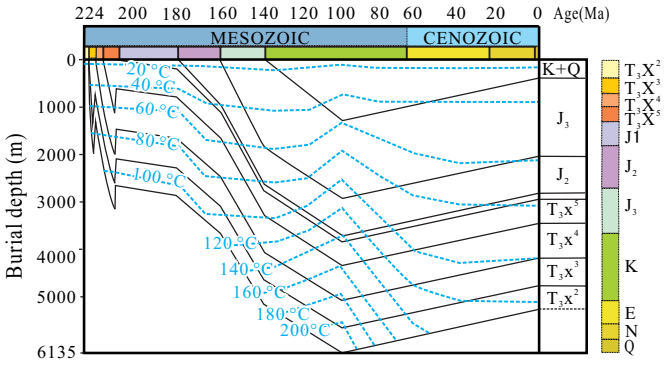

Figura 11. Burial history for well Chuanxiao565 of the WDSC.

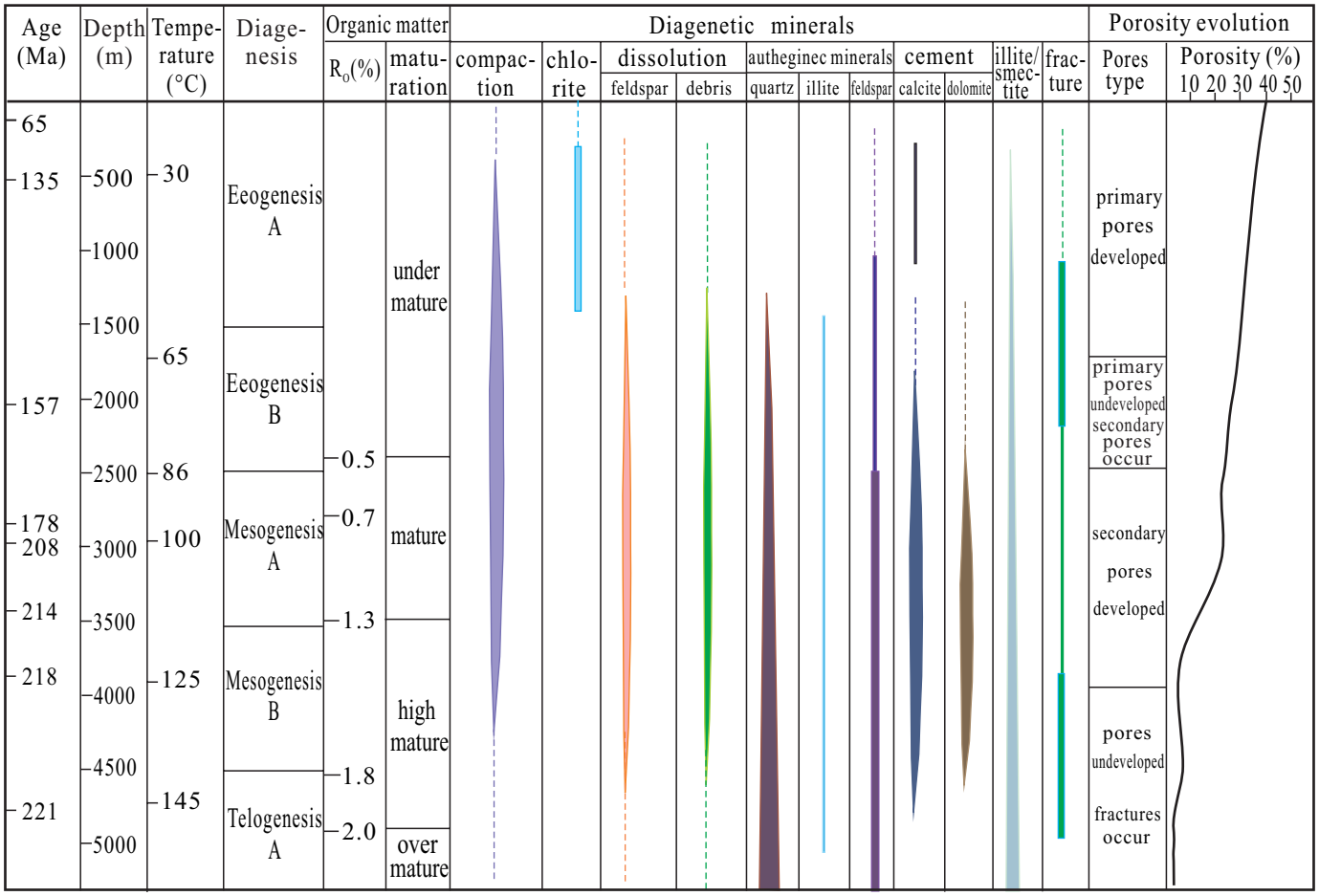

Figura 12. Diagenetic processes in the Xu2 sandstones, WSDC. R_o: vitrinite reflectance.

original sedimentation and compaction are the first order parameters to have influence on porosity. However, cementation, dissolution and the growth of authigenic minerals are also key factors for predicting the porosity evolution in the tight gas sand.

Initial porosity prediction model

Much of what happens to the sediment later during the course of diagenesis is determined by its initial properties such as mineralogical composition, grain size, porosity and permeability (Giles, 1997). Many of the initial properties depend on grain size. Especially within one lithoclass, sedimentary properties, such as grain size, sorting and clay content, control the porosity and permeability. The initial porosities of natural and artificial sandstones have been investigated by many researchers including Beard and Weyl (1973), Atkins and McBride (1992), and Scherer (1987). A decrease in porosity takes place from 42%, for extremely well sorted sand (Trask sorting coefficient: 1.1) to 28% for very poorly sorted sand (Trask sorting coefficient: 4.2) (Scherer, 1987). In the initial porosity calculation function of Beard and Weyl (1973), the initial porosity (Φ_0) is related to the sorting (S) of sands under wet surface conditions:

$$\Phi_0 = 20.91 + (22.9/S) \quad (1)$$

where initial porosity (Φ_0) is in percent of bulk volume, and sorting (S) is the Trask sorting coefficient.

The initial sedimentary properties not only control the primary porosity, but also control the sedimentary features that influence the final porosity at present. Experimental analysis shows that some positive correlation exists between grain size and porosity of the tight sands of the Xujiahe Formation (Figure13). The fine- and medium-grained sands generally have higher reservoir quality, with an average

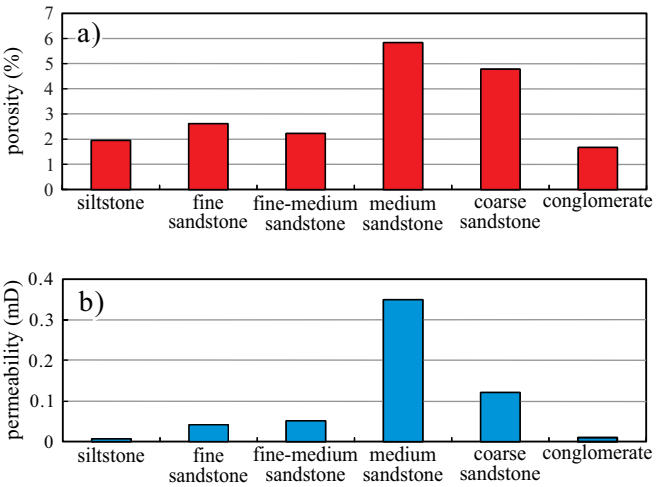

Figura 13. Histogram showing (a) porosity and (b) permeability for different lithologies of the Xujiahe Formation.

Table 3. Sorting and Trask coefficient for sandstone with different grain sizes and lithologies in the Xu2.

Granularity	Sorting	Trask coefficient	Lithology	Sorting	Trask coefficient
coarse	medium-well	1.41	quartzarenite	well	1.12
medium	medium-well	1.09	litharenite	medium-well	1.25
fine to medium	medium	1.45	sublitharenite	medium-well	1.33
fine	well	1.03	subarkose	medium	1.41

porosity of 4.35% and 5.33%, respectively. In contrast, the porosities of coarse sand, conglomerate sand and siltstone are relatively lower. The average porosities of these sands are 2.58%, 2.02% and 2.15%, respectively. Theoretically, the sand porosity is independent of grain size, but is dependent on the grain-stacking mode. However, the difference in the porosity of sands with diverse grain sizes is probably caused by differences in sorting. The analytical results from the statistics of thin sections of 150 samples from wells Xin5, Xin10, Xin11, Xin101, Fenggu21, Dayi1 and Dayi2 show that grain size and lithology type of the sand caused the differences in sand sorting (Table 3). Table 3 indicates that fine-grained sands and medium-grained sands have both low sorting coefficients, whereas coarse-grained sands have a higher coefficient. The content of detrital quartz in mineral volume also contributes to the variation of the sorting coefficient. The pure quartzarenite sandstone and litharenite have low sorting coefficients, but in contrast, sublitharenite sandstone and subarkosic sandstone have high coefficients.

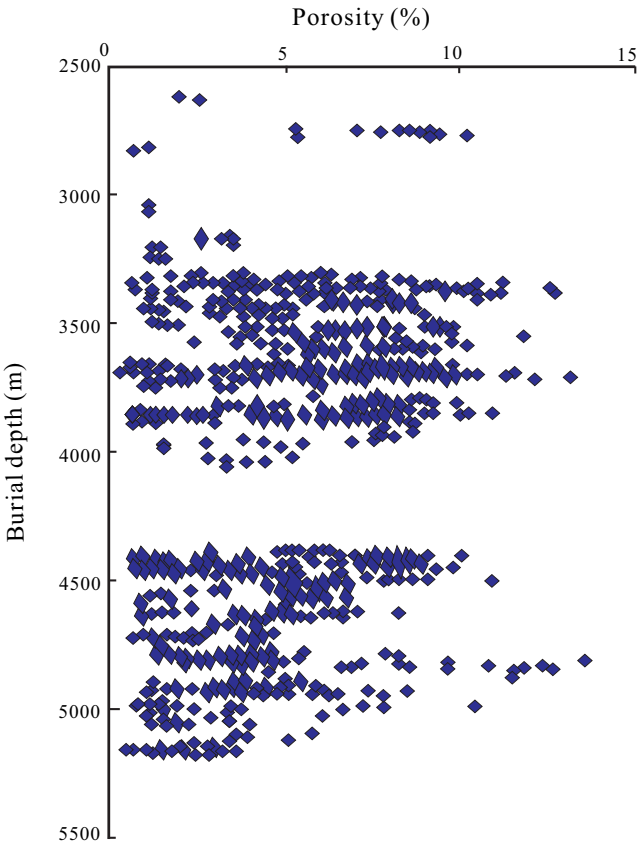

Figura 14. Porosity versus burial depth of the Xu2 sandstones, showing decreasing porosity with the increase of burial depth.

Role of compaction on porosity

Compaction is thought of as the most important parameter influencing primary porosity loss during diagenesis (Schmidt, *et al.*, 1997). Understanding the different compaction processes that change porosity, permeability and rock properties in sedimentary basins with burial and time, is both scientifically and economically important (Aagaard and Jahren, 2010). Porosity tends to decrease with increasing depth, although simple mechanical compaction (rearrangement of grains) is not the only control on porosity since the depth-porosity variation is complex and varied (Gier *et al.*, 2008). Conspicuous evidence of mechanical compaction of the tight sand of the Xujiahe Formation includes the fracturing of quartz and feldspar grains and deformation of ductile grains (mica, mud intraclasts). Chemical compaction occurred due to pressure dissolution, evidenced by grain contact suturing.

The behavior of clastic materials during sedimentation, burial and uplift has been extensively studied and presented in the literature. The early relationships for the compaction of clastic sediments relate sediment compaction with depth of burial (Athy, 1930; Magara, 1978). For instance, Athy's model relates sediment porosity, $\Phi = \Phi_0 \exp(c \cdot z)$, where Φ_0 is the initial porosity, c is an empirical constant related to the lithology of the sediment, and z is the burial depth. The porosity *vs.* depth relationship is based on a geometric exponential reconstruction. Aagaard and Jahren (2010) proposed that mechanical compaction influences sediment porosity down to depths of about 2–2.5 km (70–80 °C), below which chemical compaction dominates. In the "compaction curve" constructed by Giles (1997) the sediment porosity decreases from 40% close to the surface to 15% at a burial depth of 2500 meters. Figure 14 shows a trend to decreasing porosity with increasing burial depth for the Xu2 for 1460 data *in situ* from 33 wells. Most data originates from the western Sichuan basin, but other data were collected from the northeastern, middle and southern Sichuan basin. The distribution properties of porosity *vs.* burial depth generally indicates that porosity decreases with depth, although some porosity at deep burial depths is even higher than the porosity in relatively lower burial depths. It is shown that most reservoir porosity is lower than 10% when its burial depth reaches or exceeds 3000 meters.

Porosity loss by cementation

Compaction is limited in sandstones cemented by eogenetic silica or carbonate cementation, or chlorite coating in some samples. Although chlorite cements are only present in some samples and their contents are normally less than 1–3% of volume of the Xujiahe Formation, they are important for the reservoir quality. Observation under the microscope reveal that chlorite coatings had grown perpendicular to mineral grains or were distributed among siliceous cements. The chlorite coatings did not form when clasts are in point-to-point contact and little is observed when grains are in linear contact. This indicates that chlorite formed after compaction in the early diagenetic stage.

Porosity tends to decrease with increasing depth (Figure 14), but simple mechanical compaction is not the only control on porosity since the depth-porosity relationship is complex and varied. The maximum porosity value for a given depth interval seems to correspond to theoretical compaction curve models. However, most samples have significantly lower porosity than the theoretical maximum values. Although compaction is limited in cemented sandstones, cementation is the second most important factor for porosity loss during diagenesis. Porosity evolution obviously will not be the same in the presence of extensive cementation. This could be due to either cementation or ductile compaction or a combination of the two. Cement growth reduces the porosity since minerals grow in pore spaces, which made the primary intergranular pores, and secondary intragranular pores decrease or disappear.

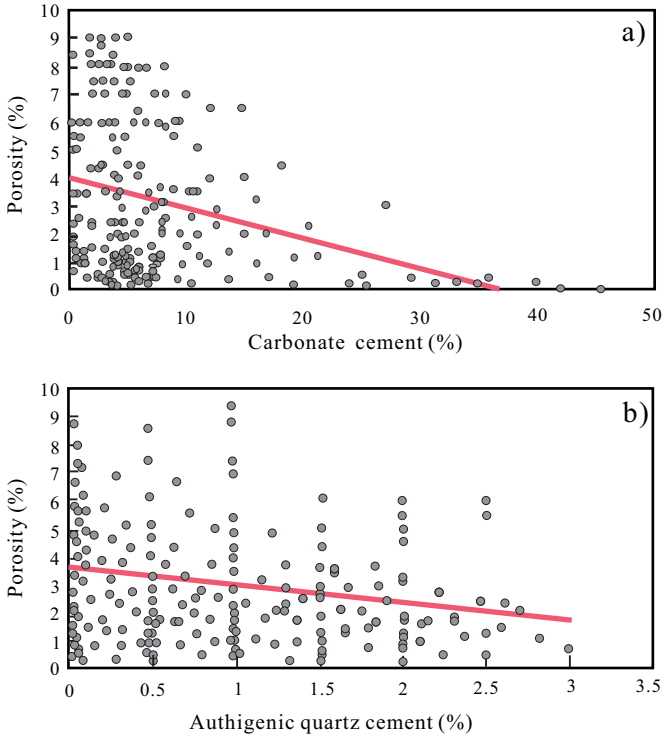

Figura 15. Cross plots of porosity versus (a) amount of carbonate cement and (b) quartz cement, showing that diagenetic cement controlls the pattern of porosity evolution in the Xu2 sandstones.

Carbonate cements and authigenic quartz are the most important cements in most of the sandstone in the Xu2, and are also important controls in the reservoir. The petrographic data revealed that there is a certain relation between porosity and cement content in the rock volume. The petrographically determined quantities of carbonate cement and quartz cement have been plotted against porosity (Figure 15). These two plots suggest that both parameters exert a significant control on porosity. Figure 15 also indicates a trend to decreasing porosity in the sandstones as the content of carbonate cements and authigenic quartz in the rock volume increases. The carbonate cement probably is the most important cement that controls the porosity, compared with the authigenic quartz. The petrographic data revealed that carbonate cement constitutes 6% of rock volume, and 80% of all the cements. Quartz constitutes 13% of cement volume on average. Silica cements are common throughout the Xujiahe Formation and almost the whole diagenetic process (Figure 16). Figure 16 shows that the average content of authigenic quartz in the rock volume increases with burial depth, which can be attested to by the investigation of thin sections. The third quartz overgrowth appears as mosaic with contacts along sutures in deeper burial depths and its content increases with burial depth (Figure 6b).

Impact of dissolution on secondary porosity

In the Xujiahe Formation, reservoir quality of the sandstones has been enhanced to various extents owing to secondary porosity development as a result of the dissolution of framework grains and K-feldspar, and also partly due to the dissolution of calcite and quartz cement. Secondary dissolution pores include pore space within dissolved framework grains and oversized pores that formed partially by the dissolution of complete grains. Dissolution of detrital grains and cements during eogenesis is presumably related to flushing by significant amounts of water (Morad *et al.*, 2000), whereas organic acids are regarded to be related to the dissolution of detrital grains and cements during mesodiagenesis (Surdam *et al.*, 1984). Such dissolution of detrital grains have resulted in oversized intragranular and moldic pores that display variable degrees of connectivity. The dissolution of early calcite cements, including predominantly non-ferroan calcite, has also resulted in portions of open, well-connected secondary intergranular pores. Though the porosity enhancement is common in sandstone of the Xujiahe Formation, only a part of the secondary pores were preserved because late-stage calcite and silica cementation filled the intragranular and intergranular dissolution pores. In some samples (Figure 8b, 8c), the pores formed by K-feldspar dissolution were partly filled by late-stage authigenic ankerite. Authigenic kaolinite, illite and quartz also precipitated and partially filled the secondary dissolution pores of K-feldspar. The preservation of secondary moldic porosity was enhanced by the presence of small amounts of evenly distributed patches of quartz and carbonate cements in the tight sandstones. In contrast to the remaining primary intergranular pores in the Xujiahe Formation, the volume of secondary dissolution residual pores takes up more of the rock volume, ranging from 1–6%, with an average of 3%. The porosity decreases systematically with increasing burial depth (Figure14), which indicates that despite the formation of secondary porosity by dissolution, diagenesis resulted in considerable destruction of reservoir quality overall.

Porosity prediction model

Based on the above depositional and diagenetic analysis, we constructed a porosity prediction model for the evolution history of the Xu2 Member tight gas sand. This historical evolution model includes

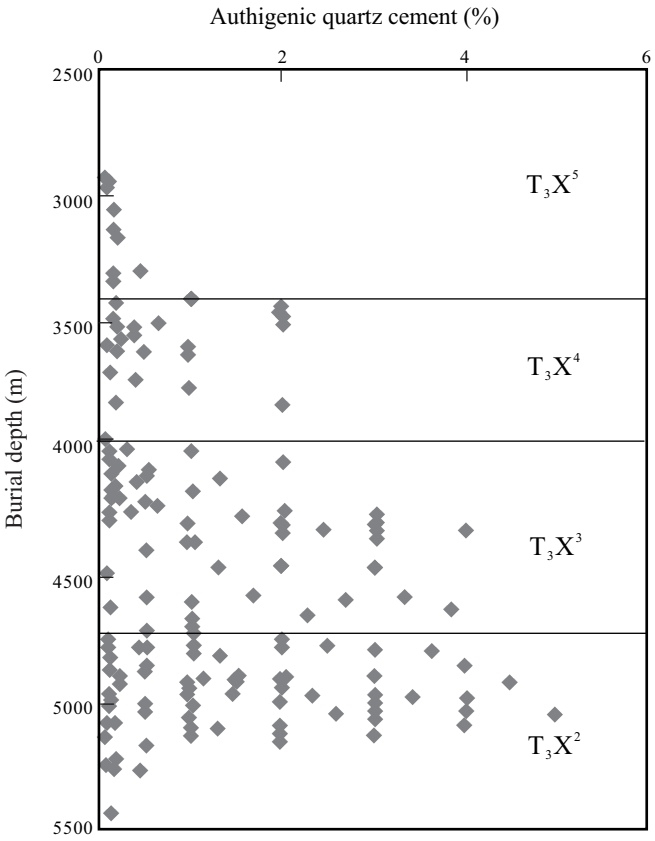

Figura 16. Cross plot of authigenic quartz cement versus burial depths for the Xu2 sandstones.

four types of parameters. Any historical porosity can be defined by Φ. The model is shown in Equation 2:

$$\Phi = \Phi_0\, e^{(-C\cdot Z)} - \Phi_{Ce} + \Phi_D \quad (2)$$

where Φ is the historical porosity in percent of bulk volume (%); Φ_0 is the initial porosity, in percent of bulk volume; C is the compaction coefficient, with values of 0.0004 m^{-1} for mudstone and 0.00033 m^{-1} for sandstone; Z is the burial depth, in meters; Φ_{Ce} is the porosity loss by cementation, which is equal to the percentage of cement content in percent of bulk volume (%); Φ_D is the porosity increase by dissolution, in percent of bulk volume (%), related to the dissolution surface ratio of total pore volume.

Because the initial porosity (Φ_0) is related to the sorting (S) of sands under wet surface conditions (Equation 1), Equation 2 can be described by Equation 3. Any historical porosity (Φ) can be defined by Equation 3.

$$\Phi = (20.91 + 22.9/S)\cdot e^{(-C\cdot Z)} - \Phi_{Ce} + \Phi_D \quad (3)$$

Porosity evolution history

Considering the depositional and diagenetic influence on porosity, the regional porosity evolution history for the Xu2 Member tight gas sand was simulated in this work through a comprehensive analysis of burial, temperature and diagenetic history (Figure 12).

Eogenesis A occurred at burial depths lower than 1500 m, and the organic matter did not matured for oil or gas generation, corresponding to the late Xu4 Member depositional age. Based on the statistics, the content of authigenic chlorite has calculated ranges from 0–8%, with an average of 4%. Due to early quartz growth restraint, the content of chlorite is basically equal to the increase of partial porosity. Mechanical compaction is out of question as the principal factor for the loss of porosity. If well-sorted, fine-grained sandstones were selected to calculate and its initial compaction coefficient of sandstone is 0.0004 m^{-1}, then the initial porosity would be decreased from 40% to 28%. The historical porosity (Φ) can be defined for Z = 0–1500 m as:

$$\Phi = \Phi_0\cdot e^{(-C\cdot Z)} + Z/1500\cdot C_C \quad (4)$$

where C_C is the content of authigenic chlorite as percent of bulk volume (%).

In the Eogenesis B, the burial depth ranged from 1500 m to 2500 m, and organic matter just entered the mature stage, corresponding to the Late Triassic. Mechanical compaction is still the major factor for the loss of primary pores, and a small quantity of secondary dissolution pores formed because of the dissolution of feldspar and rock fragments. Because the development of authigenic chlorite rims was not continuous, early quartz growth occurred. For the whole diagenetic stage, total authigenic quartz content varies from 2 to 12%, with an average of 8% of the bulk volume. Dissolution porosity represents 2–5% of the bulk volume. After Eogenesis A and B, the remaining porosity of the Xu2 Member tight gas sand generally decreased from 28% to 22%. The historical porosity (Φ) for Z=1500–2500 m can be calculated as:

$$\Phi = \Phi_0\cdot e^{(-C\cdot Z)} + C_C + (Z\text{-}1500)/(4500\text{-}1500)\cdot C_Q + (Z\text{-}1500)/(4500\text{-}1500)\cdot C_D \quad (5)$$

where, C_Q is the content of quartz growths as a percent of the bulk volume (%), and C_D is the dissolution porosity.

During the mesogenesis, the burial depth ranged from 2500–4500 m, and the organic matter reached the highly mature stage, corresponding to the middle Cretaceous. Although the compaction resulted in concave-convex with subordinate suturing contacts, compaction still exerted an influence in the loss of porosity. In addition to the authigenic quartz representing the phase II quartz growth and the dissolution of feldspar and debris, late ferroan calcite and dolomite began to occur. In this stage, a range of authigenic quartz made the content of silica cementation to increase in about 2–4%. The volume of late-stage carbonaceous cements increased from 5% to 8% percent of bulk volume. Although the dissolution was continuous, the positive alteration of the tight sand was not apparent, so the intensive compaction, cementation and authigenic minerals caused the sandstone to begin to be consolidated. At the end of the mesogenesis phase, the range of remaining porosity of the Xu2 Member tight gas sand possibly decreased by 6–10%. The historical porosity (Φ) can be calculated for Z=2500–4500 m as:

$$\Phi = \Phi_0\cdot e^{(-C\cdot Z)} + C_C + (Z\text{-}1500)/(4800\text{-}1500)\cdot C_Q + (Z\text{-}1500)/(4800\text{-}1500)\cdot C_D - (Z\text{-}2500)/(4800\text{-}2500)\cdot C_A \quad (6)$$

where, C_A is the content of late-stage carbonaceous cements, as percentage of bulk volume (%), and C_D is the dissolution porosity.

The telogenesis occurred at burial depths of more than 4500 m, with organic matter at the over mature stage with VR_o% of over 2.0%; this phase took place in a time span between the late Cretaceous and the present. Almost all diagenetic processes had weakened, with the exception of occasional chemical compaction and microfracturing. Dissolution processes almost disappeared because of the lack acidic fluids and organic matter. The remaining porosity sharply decreased, and the Xu2 Member tight sand was totally consolidated because of the previous compaction, cementation and formation of authigenic minerals. When the tight sand was buried to depths of more than 5000 m, the range of porosity generally was decreased by 2–5%. In this process, quartz growth and formation of authigenic feldspar, with occasional chemical compaction, badly destroyed the remaining pores. However, late tectonic processes, like the Yanshan movement (Jurassic to Cretaceous) and Himalayan movement (Tertiary to Quaternary), led to the intensive development of structural fractures in the tight sand. In this view, fractures actually developed during the whole diagenesis. The historical porosity (Φ) for can be calculated Z =4500 m as:

$$\Phi = \Phi_0\cdot e^{(-C\cdot Z)} + C_C - C_Q + C_D - C_A \quad (7)$$

Densification time of the tight gas sand

Three gas fields (Xinchang, Dayi and Yazihe) were chosen for the prediction of the regional porosity evolution. As for the Xu2 Member tight sand in the Xinchang and the Dayi gas fields, the sandstones are medium-grained, medium- to well-sorted lithic quartz sandstone, so the initial porosity and the compaction coefficients can be calculated at 40% and 0.0004 m^{-1}, respectively. However, the initial porosity and the compaction coefficients can be defined as 37.5% and 0.0004 m^{-1} for the Xu2 Member tight sand from the Yazihe gas field, because the lithic quartz sandstone has the property of being coarser grained, partially showing coarse sandstone. Compared to the Xinchang tight sand, the sand from Dayi gas field does not show the phenomenon of early chlorite restraining the growth of quartz. The matrix of the Dayi sand is about 1–8%, with an average content of siliceous and carbonaceous cements of 5% and 6%, respectively. The Yazihe sand has a relatively more argillaceous matrix and early poikilotopic calcite in contents of 3.7% and 3.6% of bulk volume of the sand, respectively. Considering the depositional and diagenetic influence on porosity, three different regional porosity evolution history models were constructed for the

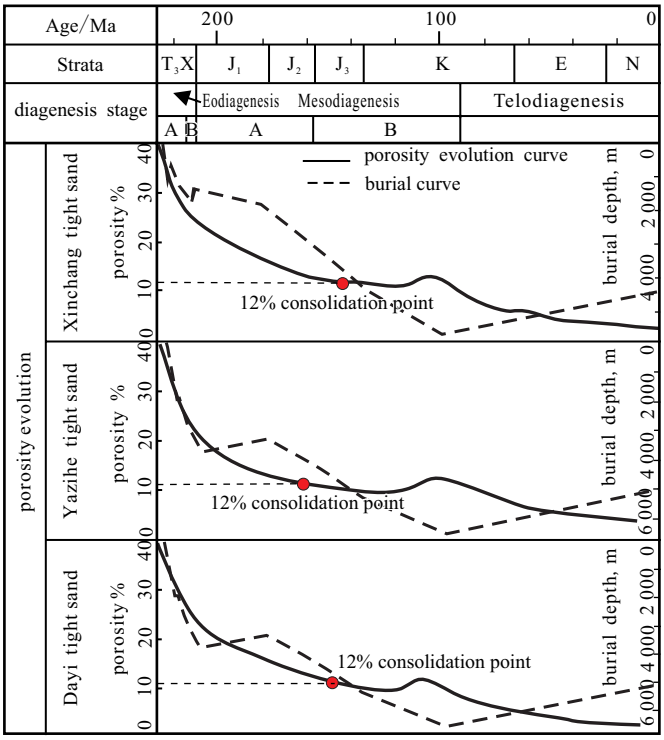

Figura 17. Porosity evolution of the Xu2 sandstones in three gas fields of the WSDC.

Xu2 Member tight gas sand through a comprehensive analysis of burial, temperature and diagenetic history. The results show that the densification time of the tight gas sand in the Xinchang, Yazihe and Dayi gas fields was during the early stage of the Late Jurassic, the early stage of the Middle Jurassic and the Late Jurassic, respectively (Figure17).

CONCLUSIONS

The Sichuan basin in southwest China is an important area for the study of a basin-centered gas system. The Upper Triassic Xujiahe Formation in the western Sichuan depression in that basin has suitable geological features for the study of porosity evolution. The sandstones of the Xu2 Member are typical tight sands with the characteristics of extremely low porosity and permeability. The primary sedimentary porosity is believed to be related to the grain size and sorting coefficient. Mechanical and chemical compaction is thought of as the most important parameter influencing primary porosity loss during diagenesis. Cementation significantly controls the quality of the reservoir. High percentages of carbonate cements and authigenic quartz in rock volume results in decreasing porosity. Reservoir quality of the sandstones was partially enhanced by the development of secondary porosity as a result of the dissolution of framework grains and K-feldspar. Diagenetic processes in the Xu2 Member tight sand occurred in five phases. Eogenesis A and Mesogenesis A and B were the most important diagenesis stages for the loss of porosity because of the intensive mechanical compaction, quartz growth and formation of carbonaceous cements. At the end of the mesogenesis, the remaining porosity of the Xu2 Member tight gas sand possibly decreased by 6–10%. From the late Cretaceous to the present, the remaining porosity sharply decreased, and the tight sand was totally consolidated. The densification time of the tight gas sand for different gas fields varied, but the main stage of sandstone consolidation could be placed from about the Middle Jurassic to the Late Jurassic.

ACKNOWLEDGMENTS

This study was funded by the China National Natural Science Foundation Programs (Grant No. 40802029 and 41072100) and the China 973 Key Foundation Research Development Project (Grant No. 2011CB201102) and China University of Petroleum (Grant No. KYJJ2012-01-02). We are grateful to the Southwest Oil Company, SINOPEC, the Chinese University of Petroleum (Beijing), the State Laboratory of Petroleum Resource and Prospecting, for providing research funding, data access and for permission to publish. We are grateful to Dr. Gustavo Murillo Muñetón who kindly reviewed a previous version of this article.

REFERENCES

Aagaard, P., Jahren, J., 2010, Special issue introduction : Compaction process–porosity, permeability and rock properties evolution in sedimentary basins: Marine and Petroleum Geology, 27, 1681-1683.

Athy, L.F., 1930, Density, Porosity and Compaction of Sedimentary Rocks: AAPG Bulletin, 4, 1-24.

Atkins, J.E., McBride, E.F., 1992, Porosity and packing of Holocene river, dune, and beach sands: AAPG Bulletin, 76, 339-355.

Beard, D.C. Weyl, P.K., 1973, Influence of texture on porosity and permeability of unconsolidated sand: AAPG Bulletin, 57,349-369.

BP World Energy Statistics, 2009, http://www.bp.com/productlanding.do?categoryId=6929ontentId=7044622/2009.

Chuhan, F.A., Kjeldstad, A., Bjorlykke, K., Hoeg, K., 2002, Porosity loss in sand by grain crushing – Experimental evidence and relevance to reservoir quality: Marine and Petroleum Geology, 19, 39-53.

Dai, J., Ni, Y., Wu, X., 2012, Tight gas in China and its significance in exploration and exploitation (in Chinese with English abstract): Petroleum Exploration and Development: 39(3), 277–284.

Dickson, J.A.D., 1965, A modified staining technique for carbonates in thin section: Nature, 205, 587.

Dutton, P.S., Robert, G.L., 2010, Diagenetic controls on evolution of porosity and permeability in lower Tertiary Wilcox sandstones from shallow to ultradeep (200-6700 m) burial: Gulf of Mexico Basin, U.S.A. Marine and Petroleum Geology, 27, 69-81.

Giles, M.R., 1997, Diagenesis: A quantitative perspective: London, Kluwer Academic Publishers, 5-8.

Gier, S., Worden, H.R., Johns, D.W., Kurzewell, H., 2008, Diagenesis and reservoir quality of Miocene sandstones in the Vienna Basin, Austria: Marine and Petroleum Geology, 25, 681-695.

Johnson, H., Fisher, M.J., 1998, North Sea plays: geological controls on hydrocarbon distribution, *in* Glennie, K.W. (ed.), Petroleum Geology of the North Sea: Basic Concepts and Recent Advances: John Wiley & Sons, 463-548.

Ketzer, J.M., Morad, S., Evans, R., Al-Aasm, I., 2002, Distribution of diageneic alterations in fluvial, deltac, and shallow marine sandstons within a sequence stratigraphic frameworks: evidence from the Mullaghmore Formation (carboniferous), NW Ireland: Journal of Sedimentary Research 72, 760-774.

Lander, R.H., Walderhaug, O., 1999, Porosity prediction through simulation of sandstone compaction and quartz cementation: AAPG Bulletin, 83, 433-449.

Law, B.E., 2002, Basin-Centered Gas Systems: AAPG Bulletin, 86(11), 1891-1919.

Li, L.T., Pang, X.Q., Xiong, L., Deng, K., Zhang, J.H., 2010, Recovery of Structural Trap Evolution by Mean of Denudation Value: A Case of Upper Triassic Xujiahe Formation Layer in Middle Section of West Sichuan Depression: Natural gas geoscience, 21(3), 441-448 (in Chinese with English abstract).

Lu, Z.X., Liu, S.B., 2009, Ultra-tight sandstone diagenesis and mechanism for the formation of relatively high-quality reservoir of Xujiahe Formation in

western Sichuan: Acta petrologica Sinica, 25(10), 2373-2383 (in Chinese with English abstract).

Luo, X., Vasseurm, G., 1992, Contributions of compaction and aquathermal pressuring to geopressure and the influence of environmental conditions: AAPG Bulletin, 76 (10), 1550–1559.

Makowitz, A., Lander, R.H.M., Milliken, K.L., 2006, Diagenetic modeling to assess the relative timing of quartz cementation and brittle grain processes during compaction, AAPG Bulletin 90, 873-885.

Magara, K., 1978, Compaction and fluid migration: Practical petroleum geology. Development in petroleum science, 9: Amsterdam: Elsevier, 313 pp.

Masters, J.A., 1979, Deep basin gas trap, western Canada: AAPG Bulletin 63(2), 151-181.

Moore, D.M., Reynolds, R.C., 1997, X-ray Diffraction and the Identification and Analysis of Clay Minerals: Oxford University Press, Oxford, 378 pp.

Morad, S., Ketzer, J.M., Ros, L.F., 2000, Spatial and temporal distribution of diagenetic alterations in siliclastic rocks: implications for mass transfer in sedimentary basins: Sedimentology, 47, 1-27.

Robinson, J.W., Shanley, W. S., 2004. Jonah Field: case study of a tight-gas fluvial reservoir. AAPG studies in Geology 52, 283 pp.

Scherer, M., 1987, Parameters Influencing Porosity in Sandstones: A Model for Sandstone Porosity Prediction: AAPG Bulletin ,71(5),485-491.

Schmidt, V., McDonald, D., Platt, R.I., 1997, Pore geometry and reservoir aspects of secondary porosity in sandstones: Bulletin of Canadian Petroleum Geology, 15, 271-290.

Song, Y., Hong, F., 2001, The geological conditions of deep-basin gas in western depression of Sichuan Basin: Petroleum exploration and development, 28(2), 11-14 (in Chinese with English abstract).

Surdam, R.C., Bose, S.W., Crossey, L.W., 1984, The chemistry of secondary porosity. In: McDonald, D.A., Surdam, R.C. (Eds.), Clastic diagenesis: AAPG Memoir 37, 127-134.

Surdam, R.C., Jiao, Z.S., Heasler, H.P., 1997, Anomalously pressured gas compartments in Cretaceous rocks of the Laramide basins of Wyoming: a new class of hydrocarbon accumulation. In: Surdam, R.C. (Ed.), Seals, Traps, and the Petroleum Systems: AAPG Memoir, 67, 199-222.

Tang, L.Z., Zhang, G.S., Zhang, X.P., An, F.S., 2004, Main control factor of forming the tight sandstone gas reservoirs in Xujiahe formation in West Sichuan basin: Natural gas industry, 24(9), 5-7 (in Chinese with English abstract).

Wang, J.Q., 2001, Early Accumulation and Late Seal - the Basic Character of Gas Reservoirs in West Sichuan Depression: Natural Gas Industry 21(1), 6-12 (in Chinese with English abstract).

Xu, Z.Y., Wu, S.H., Zhang, X.Q., Zhao, Y., Zeng, X.Y., 2008, Diagenetic reservoir facies and their evolutionary sequences of the Members 4 and 2 of Upper Triassic Xujiahe Formation in Xinchang gas field, Western Sichuan Depression: Journal of Paleogeography, 10(5), 448-458 (in Chinese with English abstract).

Yang, H.H., Li, Z.H,. 2004, Development of Geothermal Pool Deduced from Old Thermal Current Values and Denudation Quantity-By the Example of Well 100 at Chuanhe in Sichuan Basin: Sichuan geological acta, 24(3): 180-184.

Yang, K.M., 2003, Status of Oil and Gas Resources and Prospecting Potential in West Sichuan Depression: Oil and Gas Geology, 2003, 24(4), 322-326 (in Chinese with English abstract).

Zhu, R.K., Zou, C.N., Zhang, N., Wang, X.S., Cheng, R., 2008, Diagenetic fluids evolution and genetic mechanism of tight sandstone gas reservoirs in Upper Triassic Xujiahe formation in Sichuan Basin, China (n Chinese with English abstract): Science in China Series D: Earth Science, 51(9), 1340-1353.

Zou, C., Zhu, R., Liu, K., 2012, Tight gas sands reservoirs in China: characteristics and recognition criteria: Journal of Petroleum Science and Engineering, 88-89 (in Chinese with English abstract).

Zou, C., Tao, S., Zhu, R., Yuan, X., Li, W., 2009, Formation and distribution of "continuous" gas reservoirs and their giant gas province: a case from the Upper Triassic Xujiahe formation giant gas province, Sichuan Basin: Petroleum exploration and development, 36(3), 307-319 (in Chinese with English abstract).

Manuscript received: October 28, 2013
Corrected manuscript accepted: February 27, 2014
Manuscript accepted: March 10, 2014